# Non-smooth 3D Modeling of a Snake Robot with External Obstacles

Aksel Andreas Transeth*, Remco I. Leine†, Christoph Glocker†, and Kristin Y. Pettersen*
*Department of Engineering Cybernetics, NTNU, NO-7491 Trondheim, Norway
E-mail: Aksel.Andreas.Transeth@itk.ntnu.no, Kristin.Y.Pettersen@itk.ntnu.no
† IMES–Center of Mechanics, ETH Zürich, CH-8092 Zürich, Switzerland
E-mail: Remco.Leine@imes.mavt.ethz.ch, Christoph.Glocker@imes.mavt.ethz.ch

*Abstract*—In this paper we extend a non-smooth 3D mathematical model of a snake robot to also include external obstacles to enable obstacle aided locomotion. The model is based on the framework of non-smooth dynamics and convex analysis. This framework enables us to systematically and easily incorporate unilateral contact forces (from the obstacles and the ground) and isotropic friction forces based on Coulomb's law. The obstacles are shaped as vertical cylinders and we describe the contact between a link of the snake robot and an obstacle with a single, moving contact point. Hence, the effect of the link touching the obstacle is accurately described. Simulation results for a 11 link snake robot moving by the serpentine motion pattern 'lateral undulation' while pushing against obstacles are given.

*Index Terms*—Non-smooth dynamics, contact modeling

## I. INTRODUCTION

Many snakes exploit roughness in the terrain and narrow passages to move forward [1]. A locomotion system that could exhibit the same robust property of mobility would be of great help for rescue workers and maintenance personnel world wide. Rescue workers would then be able to locate and aid people trapped by collapsed buildings or mines. In addition, surveillance and maintenance of complex and possible dangerous structures could be performed by the maintenance personnel from a safe distance. A snake robot, with its highly articulated body, constitutes a locomotion system that could be able to perform the tasks mentioned above. In this paper we present a mathematical model of a snake robot which includes external obstacles, as a first step towards developing a snake robot that can exploit external obstacles and thus play an important role in search and rescue missions.

We define in this paper *obstacle aided locomotion* as snake robot locomotion where the snake robot utilizes walls or other external objects, apart from the flat ground, for means of propulsion. A snake robot moving by the principle of obstacle aided locomotion would be able to exploit the chaotic environment inside a collapsed building to move forward. Also, such locomotion will be more robust to various kinds of surfaces. Even though obstacle aided locomotion was investigated as early as in 1976 [2] and further elaborated on in [3], the subject has not been mentioned in many papers in the subsequent years apart from, for example, snake robot locomotion with pegs in [4]. The latter paper adds linear actuators along each link, increasing the complexity of the snake robot. A complete analytical model of the dynamics
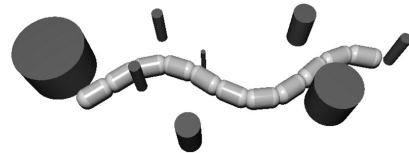


Fig. 1.    Snake robot moving by lateral undulation by pushing against cylindrical obstacles. The snake robot is moving towards the left in the picture.

of a snake robot with obstacles is important for analysis of obstacle aided locomotion. However, no such model has been found in literature.

Few mathematical models describing the 3D dynamics of snake robots have been found in literature. The first 3D model was presented in [5]. A 3D model with a compliant ground contact model, modeled as a mass-damper-spring system, has been published in [6], where a very high spring coefficient is needed to model a hard floor. In addition, it is not clear how to determine the dissipation parameters of the contact unambiguously when using a compliant model [7]. The friction force between the underside of the snake robot and the ground has usually been described by a Coulomb or viscous-like friction model [8], [9], and the Coulomb friction has most often been modeled using the sign-function [5], [8]. However, only unidirectional friction can be described by a sign-function (see Section IV-B.2). Moreover, a steep and smooth approximation of the sign-function together with the compliant contact model lead to stiff differential equations which are cumbersome to solve numerically. Hence, there is a need for a non-smooth model which correctly describes spatial Coulomb friction with stiction as well as the unilaterality of the contact.

In this paper we extend the non-smooth analytical 3D model of the snake robot presented in [10] to also include the possibility of utilizing external obstacles, shaped as vertical cylinders of any radius, for locomotion (See Fig. 1). Simulation results using the serpentine motion pattern 'lateral undulation' for obstacle aided locomotion are given. *Set-valued* force laws for the unilateral contact force and the friction force in a three-dimensional setting are described in the framework of non-smooth dynamics and convex analysis [7], [11], [12]. Hence, stick-slip transitions and impacts with the ground and obstacles are modeled as instantaneous transitions. We describe the contact between an obstacle and the surface of each link of the

snake robot with a single, *moving* contact point. This provides us with an accurate description of where the various obstacle contact forces act on the snake robot.

We choose six non-minimal absolute coordinates for each link and include the bilateral constraint forces in the joints as Lagrangian multipliers in the mathematical model. This choice of coordinates yields a constant and diagonal mass matrix, and very simple expressions for the gyroscopic forces which both are beneficial for numerical efficiency.

The paper is organized as follows. The choice of coordinates and reference frames, and the contact constraints on position level presented as gap functions, are given in Section II. Section III shows how to obtain expressions for the relative velocities, needed to find the contact and friction forces, from the gap functions. Section IV describes the non-smooth dynamics of the snake robot and Section V explains how to control the joint angles. A brief summary of the numerical treatment of the model is given in Section VI, while Section VII contains the simulation results. Concluding remarks are given in Section VIII.

## II. KINEMATICS

The kinematics of the snake robot with obstacles is presented here. From the kinematics, we develop *gap functions* for obstacle and ground contact detection. These functions are also used as a basis for calculating the contact forces.

This section will first give an overview of the coordinates used to describe the position and orientation of the snake robot. Subsequently, the gap functions for contact with external obstacles and the ground will be presented.

### A. Coordinates and Reference Frames

The snake robot consists of $n$ links that are connected by $n-1$ cardan joints, each having two degrees of freedom (DOF). The distance $L_i$ between two adjacent cardan joints equals the length of link $i$. The surface of link $i$ is defined as a cylinder of length $2L_{GS_i}$ and radius $L_{SC}$. Two half-spheres, each with radius $L_{SC}$ are mounted on each end of the cylinder, see Fig. 2. Denote the centre of the front and rear disc that constitute the ends of the cylinder as $S_{Fi}$ and $S_{Ri}$, with positions $\boldsymbol{r}_{S_{Fi}}$ and $\boldsymbol{r}_{S_{Ri}}$, respectively. Fig. 2 also depicts the earth-fixed coordinate frame $I = \left(O, \boldsymbol{e}_x^I, \boldsymbol{e}_y^I, \boldsymbol{e}_x^I\right)$ used as an approximation to an inertial frame where its centre $O$ is fixed to the ground surface and the $\boldsymbol{e}_z^I$-axis is pointing in the opposite direction of the acceleration of gravity vector $\boldsymbol{g}$. External objects (obstacles) are included in the model for the snake robot to push against during locomotion. The external object $j$ is modeled as a cylinder of radius $L_{H_j}$ and infinite height with its mid-line parallel to $\boldsymbol{e}_z^I$. The position of the point $H_j$ where the mid-line of obstacle $j$ intersects with the $\left(\boldsymbol{e}_x^I, \boldsymbol{e}_y^I\right)$-plane is denoted by $\boldsymbol{r}_{H_j}$.

The position and orientation of link $i$ are described by the *non-minimal absolute* coordinates

$$\boldsymbol{q}_i = \begin{bmatrix} {}_I\boldsymbol{r}_{G_i} \\ \boldsymbol{p}_i \end{bmatrix} \in \mathbb{R}^7, \qquad (1)$$
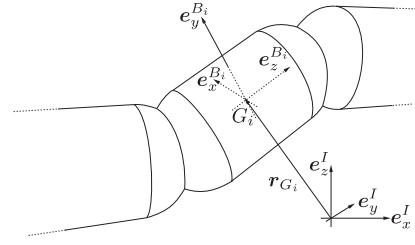


Fig. 2. Link $i$ and reference frames.

where ${}_I\boldsymbol{r}_{G_i} \in \mathbb{R}^3$ is the position of the centre of gravity of link $i$ and the vector $\boldsymbol{p}_i = \begin{bmatrix} e_{i_0} & \boldsymbol{e}_i^{\mathrm{T}} \end{bmatrix}^{\mathrm{T}}$, where $\boldsymbol{e}_i^{\mathrm{T}} = \begin{bmatrix} e_{i_1} & e_{i_2} & e_{i_3} \end{bmatrix}$, contains the four Euler parameters used to describe the rotation. The Euler parameters form a unit quaternion vector with the constraint $\boldsymbol{p}_i^{\mathrm{T}}\boldsymbol{p}_i = 1$. The coordinates are *non-minimal* because each link is described with 6 coordinates, *absolute* because the position and orientation of link $i$ is given directly relative to the inertial frame $I$. The velocity of link $i$ is given by

$$\boldsymbol{u}_i = \begin{bmatrix} {}_I\boldsymbol{v}_{G_i} \\ {}_{B_i}\boldsymbol{\omega}_{IB_i} \end{bmatrix} \in \mathbb{R}^6 \qquad (2)$$

where ${}_I\boldsymbol{v}_{G_i}$ is the translational velocity of the CG of link $i$ which is ${}_I\boldsymbol{v}_{G_i} = {}_I\dot{\boldsymbol{r}}_{G_i}$ when it exists (i.e. for impact free motion). Moreover, ${}_{B_i}\boldsymbol{\omega}_{IB_i}$ is the angular velocity of frame $B_i$ relative to frame $I$, given in frame $B_i$. The transformation ${}_I\boldsymbol{r} = \mathbf{R}_{B_i}^I {}_{B_i}\boldsymbol{r}$ can be performed with the rotation matrix $\mathbf{R}_{B_i}^I = \mathbf{H}_i\bar{\mathbf{H}}_i$ where

$$\mathbf{H}_i = \begin{bmatrix} -\boldsymbol{e}_i & \tilde{\boldsymbol{e}}_i + e_{i_0}\mathbf{I} \end{bmatrix}, \ \bar{\mathbf{H}}_i = \begin{bmatrix} -\boldsymbol{e}_i & -\tilde{\boldsymbol{e}}_i + e_{i_0}\mathbf{I} \end{bmatrix}, \quad (3)$$

and the superscript $\tilde{}$ denotes the skew-symmetric form of $\boldsymbol{e}$. The time-derivative of the rotation matrix is found from [13] as

$$\dot{\mathbf{R}}_{B_i}^I = \mathbf{R}_{B_i}^I {}_{B_i}\tilde{\boldsymbol{\omega}}_{IB_i}. \qquad (4)$$

The generalised coordinates (positions and orientation) and velocities of all links are gathered in the vectors $\boldsymbol{q} = \begin{bmatrix} \boldsymbol{q}_1^{\mathrm{T}} & \cdots & \boldsymbol{q}_n^{\mathrm{T}} \end{bmatrix}^{\mathrm{T}}$ and $\boldsymbol{u} = \begin{bmatrix} \boldsymbol{u}_1^{\mathrm{T}} & \cdots & \boldsymbol{u}_n^{\mathrm{T}} \end{bmatrix}^{\mathrm{T}}$.

### B. Gap Functions for Contact with External Objects

We begin this section by giving a short description of what a gap function is and what it is used for. Then, we introduce the gap functions for the contact with external objects.

Consider two convex rigid bodies 1 and 2. Now, we want to determine whether Body 1 is in contact with Body 2. This can be achieved by determining whether the minimal distance between the two bodies is equal to zero. The function that gives us the minimal distance is called a *gap function* [14] and the point on Body 1 that is closest to Body 2 is called a (possible) contact point. Apart from determining if two rigid bodies are in contact, the gap function will also be used as a basis for calculating the direction and size of the forces involved in the contact.

Link $i$ can, at each time-instance, only touch a convex obstacle $j$ at one point, resulting in a contact point that may move across the entire surface of a link. Hence, by inspecting
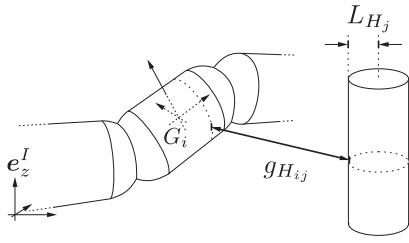
Fig. 3. Illustration of the shortest distance between link $i$ and obstacle $j$.



Fig. 4. Surfaces (solid-drawn circles) on snake robot that constitute the contact between the robot and the ground.

the shape of the surface of a link, we need to consider the distances between two cylinders, and a cylinder and a sphere to calculate the shortest distance (i.e. the gap functions) between the link and the obstacle, see Fig. 3.

*1) Cylinder - Cylinder Contact:* If the part of link $i$ which is shaped as a cylinder is closest to the obstacle (also being a cylinder), then the gap function for object contact is defined as the distance between these two cylinders. The distance between two cylinders equals the distance between their mid-lines minus the sum of their radii. The normal vector to the mid-lines of both the obstacle $j$ and the link $i$ cylinder is

$$ \boldsymbol{n}_{ij} = \frac{\boldsymbol{e}_z^I \times \boldsymbol{e}_z^{B_i}}{\|\boldsymbol{e}_z^I \times \boldsymbol{e}_z^{B_i}\|}. \tag{5} $$

The shortest distance between the two mid-lines can now be found as

$$ d_{ij} = \left( \boldsymbol{r}_{G_i} - \boldsymbol{r}_{H_j} \right)^{\mathrm{T}} \boldsymbol{n}_{ij}, \tag{6} $$

Hence, the gap function is

$$ g_{H_{ij}} = |d_{ij}| - \left( L_{H_j} + L_{SC} \right). \tag{7} $$

*2) Cylinder - Sphere Contact:* If one of the two half-spheres of link $i$ is closest to obstacle $j$, then the gap function between the link and the obstacle is

$$ g_{H_{ij}} = \|\boldsymbol{r}_{H_j S_i}\| - \left( L_{H_j} + L_{SC} \right), \tag{8} $$

where $\boldsymbol{r}_{H_j S_i}$ is a vector from $H_j$ to the *projection of either $S_{Fi}$ or $S_{Ri}$ onto the $\left( \boldsymbol{e}_x^I, \boldsymbol{e}_y^I \right)$-plane* depending on which end of the link is closest to the obstacle. Hence, it holds that

$$ \boldsymbol{r}_{H_j S_i} = \begin{cases} \boldsymbol{r}_{H_j S_{Fi}} & \text{, front part of link } i \text{ is closest,} \\ \boldsymbol{r}_{H_j S_{Ri}} & \text{, rear part of link } i \text{ is closest,} \end{cases} \tag{9} $$

where

$$ \boldsymbol{r}_{H_j S_{Fi}} = \mathbf{A}_{xy} \left( \boldsymbol{r}_{G_i} + \boldsymbol{r}_{G_i S_{Fi}} \right) - \boldsymbol{r}_{H_j}, \tag{10} $$

$$ \boldsymbol{r}_{H_j S_{Ri}} = \mathbf{A}_{xy} \left( \boldsymbol{r}_{G_i} + \boldsymbol{r}_{G_i S_{Ri}} \right) - \boldsymbol{r}_{H_j}, \tag{11} $$

with $\boldsymbol{r}_{G_i S_{Fi}} = L_{GS_i} \boldsymbol{e}_z^{B_i}$, $\boldsymbol{r}_{G_i S_{Ri}} = -L_{GS_i} \boldsymbol{e}_z^{B_i}$, and $\mathbf{A}_{xy} = \operatorname{diag} \left( [1, 1, 0] \right)$.

*3) Vector of Gap functions for Contact with External Objects:* We now gather the gap functions $g_{H_{ij}}$ for all $n$ links and $\nu$ obstacles in the vector

$$ \boldsymbol{g}_H = \begin{bmatrix} g_{H_{11}} \cdots g_{H_{n1}} & g_{H_{12}} \cdots g_{H_{n2}} \cdots g_{H_{1\nu}} \cdots g_{H_{n\nu}} \end{bmatrix}^{\mathrm{T}} \tag{12} $$

where the elements $g_{H_{ij}}$ are found from either (7) or (8) depending on which part of link $i$ is closest to obstacle $j$.
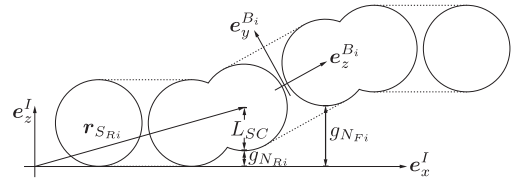
*C. Gap Functions for Unilateral Constraints*

The gap functions for the distance between the ground and the front and rear end-sphere surfaces are illustrated in Fig. 4 and are written as (see [10] for a more thorough description)

$$ g_{N_{Fi}} = \left( \boldsymbol{r}_{S_{Fi}} \right)^{\mathrm{T}} \boldsymbol{e}_z^I - L_{SC}, \; g_{N_{Ri}} = \left( \boldsymbol{r}_{S_{Ri}} \right)^{\mathrm{T}} \boldsymbol{e}_z^I - L_{SC}, \tag{13} $$

where $\boldsymbol{r}_{S_{Fi}} = \boldsymbol{r}_{G_i} + L_{GS_i} \boldsymbol{e}_z^{B_i}$, $\boldsymbol{r}_{S_{Ri}} = \boldsymbol{r}_{G_i} - L_{GS_i} \boldsymbol{e}_z^{B_i}$. The gap functions are gathered in the vector

$$ \boldsymbol{g}_N = \begin{bmatrix} g_{N_{F1}} & \cdots & g_{N_{Fn}} & g_{N_{R1}} & \cdots & g_{N_{Rn}} \end{bmatrix}^{\mathrm{T}}. \tag{14} $$

## III. CONTACT CONSTRAINTS ON VELOCITY LEVEL

In this section we calculate the relative velocities between the snake robot, and the obstacles and the ground, by taking the time-derivative (when it exists) of the appurtenant gap functions. The relative velocities are needed to set up the set-valued contact forces for the closed contacts [15]. The relative velocities concerned with the external obstacles are introduced and detailed in this paper, while the remaining relative velocities are included for the paper to be self-contained and are more thoroughly described in [10].

*A. Unilateral Contact - Obstacle Contact*

The contact between link $i$ and obstacle $j$ is modeled as an unilateral contact. To calculate the contact force, the relative velocity $\gamma_{H_{ij}} := \dot{g}_{H_{ij}}$ between obstacle $j$ and the point on link $i$ closest to the obstacle needs to be found. This is obtained from the gap functions defined in Section II-B. As for the calculations of the gap functions, the relative velocity $\gamma_{H_{ij}}$ is dependent on which part of the link is closest to the obstacle.

*1) Cylinder - Cylinder Contact:* If the cylinder part of link $i$ is closest to obstacle $j$, then the gap function is given by (7) and the relative velocity $\gamma_{H_{ij}} := \dot{g}_{H_{ij}}$ can be written as

$$ \gamma_{H_{ij}} = \left( \dot{\boldsymbol{r}}_{G_i}^{\mathrm{T}} \boldsymbol{n}_{ij} + \left( \boldsymbol{r}_{G_i} - \boldsymbol{r}_{H_j} \right)^{\mathrm{T}} \dot{\boldsymbol{n}}_{ij} \right) \operatorname{sign}(d_{ij}) \tag{15} $$

where $\boldsymbol{n}_{ij}$ and $d_{ij}$ are found from (5) and (6), respectively. Define $\| \cdot \| := \| \cdot \|_2$ and let us consider

$$ {}_I \dot{\boldsymbol{n}}_{ij} := -\frac{\frac{\mathrm{d}}{\mathrm{d}t} \|{}_I \boldsymbol{e}_z^I \times {}_I \boldsymbol{e}_z^{B_i}\|}{\|{}_I \boldsymbol{e}_z^I \times {}_I \boldsymbol{e}_z^{B_i}\|^2} \left( {}_I \boldsymbol{e}_z^I \times {}_I \boldsymbol{e}_z^{B_i} \right) + \frac{\frac{\mathrm{d}}{\mathrm{d}t} \left( {}_I \boldsymbol{e}_z^I \times {}_I \boldsymbol{e}_z^{B_i} \right)}{\|{}_I \boldsymbol{e}_z^I \times {}_I \boldsymbol{e}_z^{B_i}\|}, \tag{16} $$

where

$$ \frac{\mathrm{d}}{\mathrm{d}t} \left( {}_I \boldsymbol{e}_z^I \times {}_I \boldsymbol{e}_z^{B_i} \right) = -{}_I \tilde{\boldsymbol{e}}_z^I \boldsymbol{R}_{B_i}^I {}_{B_i} \tilde{\boldsymbol{e}}_z^{B_i} {}_{B_i} \boldsymbol{\omega}_{IB_i}, \tag{17} $$

and

$$\frac{\mathrm{d}}{\mathrm{d}t}\|_I\boldsymbol{e}_z^I \times {}_I\boldsymbol{e}_z^{B_i}\| = \frac{-\left({}_I\boldsymbol{e}_z^{B_i}\right)^\mathrm{T} \mathbf{A}_{xy}\mathbf{R}_{B_i\,B_i}^I\tilde{\boldsymbol{e}}_z^{B_i}{}_{B_i}\boldsymbol{\omega}_{IB_i}}{\|_I\boldsymbol{e}_z^I \times {}_I\boldsymbol{e}_z^{B_i}\|}. \quad (18)$$

Substitution of the above results into (15) yields

$$\gamma_{H_{ij}} = \boldsymbol{w}_{H_{ij}}^\mathrm{T}\boldsymbol{u}_i \quad (19)$$

with

$$\boldsymbol{w}_{H_{ij}} = \mathrm{sign}(d_{ij}) \cdot \left[ \left({}_I\boldsymbol{n}_{ij}\right)^\mathrm{T} \quad \boldsymbol{c}_{ij}^\mathrm{T}\mathbf{R}_{B_i\,B_i}^I\tilde{\boldsymbol{e}}_z^{B_i} \right]^\mathrm{T} \quad (20)$$

and

$$\boldsymbol{c}_{ij}^\mathrm{T} = \frac{\left({}_I\boldsymbol{r}_{G_i} - {}_I\boldsymbol{r}_{H_j}\right)^\mathrm{T}}{\|_I\boldsymbol{e}_z^I \times {}_I\boldsymbol{e}_z^{B_i}\|} \left( \frac{{}_I\boldsymbol{n}_{ij}\left({}_I\boldsymbol{e}_z^{B_i}\right)^\mathrm{T}\mathbf{A}_{xy}}{\|_I\boldsymbol{e}_z^I \times {}_I\boldsymbol{e}_z^{B_i}\|} - {}_I\tilde{\boldsymbol{e}}_z^I \right). \quad (21)$$

The motivation to write the relative velocity in the form (19) is that the vector $\boldsymbol{w}_{H_{ij}} \in \mathbb{R}^6$ constitutes the generalised force direction of the contact force between obstacle $j$ and link $i$.

*2) Cylinder - Sphere Contact:* The gap function (8) is employed to define the relative velocity $\gamma_{H_{ij}} := \dot{g}_{H_{ij}}$ when one of the two half-spheres on link $i$ is closest to the obstacle $j$. To find $\gamma_{H_{ij}}$, let us first consider the vector giving the shortest distance from obstacle $j$ to the centre of one of the end spheres of link $i$

$$\begin{aligned} {}_I\boldsymbol{r}_{H_jS_i} &= {}_I\boldsymbol{r}_{S_i} - \left({}_I\boldsymbol{r}_{H_j} + \mathbf{A}_z\,{}_I\boldsymbol{r}_{G_iS_i}\right) \\ &= \left({}_I\boldsymbol{r}_{G_i} + \mathbf{R}_{B_i\,B_i}^I\boldsymbol{r}_{G_iS_i}\right) - {}_I\boldsymbol{r}_{H_j} \quad (22) \\ &\quad - \mathbf{A}_z\left({}_I\boldsymbol{r}_{G_i} + \mathbf{R}_{B_i\,B_i}^I\boldsymbol{r}_{G_iS_i}\right), \end{aligned}$$

where the point $S_i$ is either $S_{Fi}$ or $S_{Ri}$ depending on which end of the link is closest to the obstacle, and $\mathbf{A}_z = \mathrm{diag}([0,0,1])$. We also need the derivative

$$_I\dot{\boldsymbol{r}}_{H_jS_i} = \mathbf{A}_{xy}\left({}_I\dot{\boldsymbol{r}}_{G_i} - \mathbf{A}_{xy}\mathbf{R}_{B_i\,B_i}^I\tilde{\boldsymbol{r}}_{G_iS_i\,B_i}\boldsymbol{\omega}_{IB_i}\right). \quad (23)$$

We find the relative velocity between obstacle $j$ and the point closest to the obstacle on the front or rear sphere of link $i$ as

$$\gamma_{H_{ij}} = \boldsymbol{w}_{H_{ij}}^\mathrm{T}\boldsymbol{u}_i, \quad (24)$$

where

$$\boldsymbol{w}_{H_{ij}}^\mathrm{T} = \frac{{}_I\boldsymbol{r}_{H_jS_i}^\mathrm{T}}{\|_I\boldsymbol{r}_{H_jS_i}\|}\left[\mathbf{A}_{xy} \quad -\mathbf{A}_{xy}\,\mathbf{R}_{B_i\,B_i}^I\tilde{\boldsymbol{r}}_{G_iS_i}\right], \quad (25)$$

$\boldsymbol{r}_{H_jS_i}$ is defined in (9), and

$$\boldsymbol{r}_{G_iS_i} = \begin{cases} \boldsymbol{r}_{G_iS_{Fi}} & \text{, front part of link } i \text{ is closest,} \\ \boldsymbol{r}_{G_iS_{Ri}} & \text{, rear part of link } i \text{ is closest.} \end{cases} \quad (26)$$

*3) Vector of Relative Velocities for the External Objects:* We now gather the relative velocities $\gamma_{H_{ij}}$ for all $n$ links and $\nu$ obstacles in the vector

$$\boldsymbol{\gamma}_H = \mathbf{W}_H^\mathrm{T}\boldsymbol{u} \quad (27)$$

where

$$\boldsymbol{\gamma}_H = \left[\gamma_{H_{11}}\cdots\gamma_{H_{n1}}\gamma_{H_{12}}\cdots\gamma_{H_{n2}}\cdots\gamma_{H_{1\nu}}\cdots\gamma_{H_{n\nu}}\right]^\mathrm{T}, \quad (28)$$

$$\mathbf{W}_H = \left[\mathbf{W}_{H_1} \quad \cdots \quad \mathbf{W}_{H_\nu}\right], \quad (29)$$

and

$$\mathbf{W}_{H_j} = \begin{bmatrix} \boldsymbol{w}_{H_{1j}} & \mathbf{0}_{6\times1} & \cdots & \mathbf{0}_{6\times1} \\ \mathbf{0}_{6\times1} & \ddots & & \vdots \\ \vdots & & \ddots & \mathbf{0}_{6\times1} \\ \mathbf{0}_{6\times1} & \cdots & \mathbf{0}_{6\times1} & \boldsymbol{w}_{H_{nj}} \end{bmatrix} \in \mathbb{R}^{6n\times n}. \quad (30)$$

Depending on which part of the link is closest to the obstacle, $\boldsymbol{w}_{H_{ij}}$ is obtained from either (20) or (25).

*B. Unilateral Contact - Ground Contact*

The relative velocities between the snake robot and the ground will be presented. These velocities include both relative velocities along the vertical $\boldsymbol{e}_z^I$-axis, and the tangential relative velocities along the $\boldsymbol{e}_x^I$- and $\boldsymbol{e}_y^I$-axis.

*1) Relative Velocities Along $\boldsymbol{e}_z^I$:* The relative velocities between the front and rear part of link $i$ and the ground along the $\boldsymbol{e}_z^I$-axis are defined as $\gamma_{N_{Fi}} := \dot{g}_{N_{Fi}}$ and $\gamma_{N_{Ri}} := \dot{g}_{N_{Ri}}$, respectively (if they exist) [15]. The relative velocities for the front and rear part of link $i$ are

$$\gamma_{N_{Qi}} = (\boldsymbol{w}_{N_{Qi}})^\mathrm{T}\boldsymbol{u}_i \quad (31)$$

where

$$\boldsymbol{w}_{N_{Qi}} = \left[ ({}_I\boldsymbol{e}_z^I)^\mathrm{T} \quad -({}_I\boldsymbol{e}_z^I)^\mathrm{T}\mathbf{R}_{B_i\,B_i}^I\tilde{\boldsymbol{r}}_{G_iS_{Qi}}^{B_i} \right]^\mathrm{T}, \quad (32)$$

for $Q = F, R$. A vector gathering all $\gamma_{N_{Fi}}$ and $\gamma_{N_{Ri}}$ is

$$\boldsymbol{\gamma}_N = \mathbf{W}_N^\mathrm{T}\boldsymbol{u}, \quad (33)$$

where $\boldsymbol{\gamma}_N = \left[\gamma_{N_{F1}} \quad \cdots \quad \gamma_{N_{Fn}} \quad \gamma_{N_{R1}} \quad \cdots \quad \gamma_{N_{Rn}}\right]^\mathrm{T}$, $\mathbf{W}_N = \left[\mathbf{W}_{N_F} \quad \mathbf{W}_{N_R}\right] \in \mathbb{R}^{6n\times 2n}$, and $\mathbf{W}_{N_Q}$ is given similarly to (30) by replacing all $\boldsymbol{w}_{H_{ij}}$ with $\boldsymbol{w}_{N_{Qi}}$ for $Q = F, R$, and $i = 1, \ldots, n$.

*2) Tangential Relative Velocities:* The relative velocities between the front part of link $i$ and the ground along the $\boldsymbol{e}_x^I$- and $\boldsymbol{e}_y^I$-axis are denoted by $\gamma_{T_{Fxi}}$ and $\gamma_{T_{Fyi}}$, respectively. The same notation principle applies for $\gamma_{T_{Rxi}}$ and $\gamma_{T_{Ryi}}$. The tangential relative velocities are found as

$$\gamma_{T_{F\zeta i}} = (\boldsymbol{w}_{T_{F\zeta i}})^\mathrm{T}\boldsymbol{u}_i, \quad \gamma_{T_{R\zeta i}} = (\boldsymbol{w}_{T_{R\zeta i}})^\mathrm{T}\boldsymbol{u}_i, \quad (34)$$

where

$$\boldsymbol{w}_{T_{F\zeta i}} = \left[ ({}_I\boldsymbol{e}_\zeta^I)^\mathrm{T} \quad -({}_I\boldsymbol{e}_\zeta^I)^\mathrm{T}\mathbf{R}_{B_i\,B_i}^I\tilde{\boldsymbol{e}}_z^{B_i}L_{GS_i} \right]^\mathrm{T}, \quad (35)$$

$$\boldsymbol{w}_{T_{R\zeta i}} = \left[ ({}_I\boldsymbol{e}_\zeta^I)^\mathrm{T} \quad ({}_I\boldsymbol{e}_\zeta^I)^\mathrm{T}\mathbf{R}_{B_i\,B_i}^I\tilde{\boldsymbol{e}}_z^{B_i}L_{GS_i} \right]^\mathrm{T}, \quad (36)$$

for $\zeta = x, y$.

The tangential relative velocities for the front and rear part of link $i$ are

$$\boldsymbol{\gamma}_{T_{Qi}} = \mathbf{W}_{T_{Qi}}^\mathrm{T}\boldsymbol{u}_i, \quad \mathbf{W}_{T_{Qi}} = \left[\boldsymbol{w}_{T_{Qxi}} \quad \boldsymbol{w}_{T_{Qyi}}\right] \quad (37)$$

for $Q = F, R$, where $\boldsymbol{\gamma}_{T_{Qi}} = \left[\gamma_{T_{Qxi}} \quad \gamma_{T_{Qyi}}\right]^\mathrm{T}$.

We gather the vectors $\boldsymbol{\gamma}_{T_{Fi}}$ and $\boldsymbol{\gamma}_{T_{Ri}}$ in the vector

$$\boldsymbol{\gamma}_T = \mathbf{W}_T^\mathrm{T}\boldsymbol{u}, \quad (38)$$

with $\gamma_T = \begin{bmatrix} \gamma_{T_{F1}}^{\mathrm{T}} & \cdots & \gamma_{T_{Fn}}^{\mathrm{T}} & \gamma_{T_{R1}}^{\mathrm{T}} & \cdots & \gamma_{T_{Rn}}^{\mathrm{T}} \end{bmatrix}^{\mathrm{T}}$, $\mathbf{W}_T = \begin{bmatrix} \mathbf{W}_{T_F} & \mathbf{W}_{T_R} \end{bmatrix} \in \mathbb{R}^{6n \times 4n}$, and $\mathbf{W}_{T_F}$, $\mathbf{W}_{T_R}$ are found similarly to (30) by replacing the zero-vectors with $\mathbf{0}_{6 \times 2}$ and replacing the vectors $\boldsymbol{w}_{H_{ij}}$ with the matrices $\mathbf{W}_{T_{Fi}}$, $\mathbf{W}_{T_{Ri}}$, respectively.

## C. Bilateral Constraints - Joints

Let $g_{J_{\chi i}}$, $\chi = x, y, z$, be the translational gaps in the joint between link $i$ and link $i+1$. Let $g_{J_{\phi i}}$ be the rotational 'gap'. Hence, in the absence of numerical errors we have that $g_{J_{\chi i}} = g_{J_{\phi i}} = 0$ (see [10]). The relative velocities for the translational gap between link $i$ and link $i+1$ are defined as $\gamma_{J i_{\chi}} := \dot{g}_{J_{\chi i}}$ for $i = 1, \ldots, n-1$ and $\chi = x, y, z$. We find that

$$\gamma_{J_{\chi i}} = \boldsymbol{w}_{J_{\chi i}}^{\mathrm{T}} \begin{bmatrix} \boldsymbol{u}_i \\ \boldsymbol{u}_{i+1} \end{bmatrix}, \tag{39}$$

where

$$\boldsymbol{w}_{J_{\chi i}} = \begin{bmatrix} ({}_I \boldsymbol{e}_{\chi}^I) \\ -\left( ({}_I \boldsymbol{e}_{\chi}^I)^{\mathrm{T}} \frac{L_i}{2} \mathbf{R}_{B_i}^I {}_{B_i} \tilde{\boldsymbol{e}}_z^{B_i} \right)^{\mathrm{T}} \\ -({}_I \boldsymbol{e}_{\chi}^I) \\ -\left( ({}_I \boldsymbol{e}_{\chi}^I)^{\mathrm{T}} \frac{L_{i+1}}{2} \mathbf{R}_{B_{i+1}}^I {}_{B_{i+1}} \tilde{\boldsymbol{e}}_z^{B_{i+1}} \right)^{\mathrm{T}} \end{bmatrix}. \tag{40}$$

The relative velocity for the rotational gap is defined as $\gamma_{J_{\phi i}} := \dot{g}_{J_{\phi i}}$ for $i = 1, \ldots, n-1$. Hence, it holds that

$$\gamma_{J_{\phi i}} = \boldsymbol{w}_{J_{\phi i}}^{\mathrm{T}} \begin{bmatrix} \boldsymbol{u}_i \\ \boldsymbol{u}_{i+1} \end{bmatrix}, \tag{41}$$

where

$$\boldsymbol{w}_{J_{\phi i}} = \begin{bmatrix} \mathbf{0}_{3 \times 1} \\ -\left( \mathbf{R}_{B_i}^I {}_{B_i} \tilde{\boldsymbol{e}}_y^{B_i} \right)^{\mathrm{T}} \left( {}_I \boldsymbol{e}_x^{B_{i+1}} \right) \\ \mathbf{0}_{3 \times 1} \\ -\left( \mathbf{R}_{B_{i+1}}^I {}_{B_{i+1}} \tilde{\boldsymbol{e}}_x^{B_{i+1}} \right)^{\mathrm{T}} \left( {}_I \boldsymbol{e}_y^{B_i} \right) \end{bmatrix}. \tag{42}$$

Using $\boldsymbol{\gamma}_{J_i} = \begin{bmatrix} \gamma_{J_{xi}} & \gamma_{J_{yi}} & \gamma_{J_{zi}} & \gamma_{J_{\phi i}} \end{bmatrix}^{\mathrm{T}}$, all the relative velocities concerned with the bilateral constraints are gathered as

$$\boldsymbol{\gamma}_J = \mathbf{W}_J^{\mathrm{T}} \boldsymbol{u}, \tag{43}$$

where $\boldsymbol{\gamma}_J = \begin{bmatrix} \boldsymbol{\gamma}_{J_1}^{\mathrm{T}} & \cdots & \boldsymbol{\gamma}_{J_{n-1}}^{\mathrm{T}} \end{bmatrix}^{\mathrm{T}}$,

$$\mathbf{W}_J = \begin{bmatrix} \mathbf{W}_{J1}^{\mathrm{T}} & \mathbf{0}_{4 \times 6} & \cdots & \mathbf{0}_{4 \times 6} \\ \mathbf{0}_{4 \times 6} & \mathbf{W}_{J2}^{\mathrm{T}} & & \mathbf{0}_{4 \times 6} \\ \vdots & & \ddots & \mathbf{0}_{4 \times 6} \\ \mathbf{0}_{4 \times 6} & \cdots & \mathbf{0}_{4 \times 6} & \mathbf{W}_{Jn-1}^{\mathrm{T}} \end{bmatrix}^{\mathrm{T}} \in \mathbb{R}^{6n \times 4(n-1)} \tag{44}$$

and $\mathbf{W}_{Ji} = \begin{bmatrix} \boldsymbol{w}_{Ji_x} & \boldsymbol{w}_{Ji_y} & \boldsymbol{w}_{Ji_z} & \boldsymbol{w}_{Ji_\phi} \end{bmatrix} \in \mathbb{R}^{12 \times 4}$ for $i = 1, \ldots, n-1$.

## IV. NON-SMOOTH DYNAMICS

The starting point for describing the dynamics of the snake robot is the *equality of measures* as introduced in [16]. The equality of measures includes the equations of motion for impact free motion as well as the impact equations, which give rise to impulsive behaviour [14]. In this section, we employ all the previous results to find the various components of the equality of measures.

## A. The System Dynamics as the Equality of Measures

The equality of measures describes the dynamics of the snake robot within the context of non-smooth dynamics. Velocity jumps, usually associated with impacts, are modeled to occur instantaneously. By considering the velocity to be a function $t \mapsto \boldsymbol{u}(t)$ of locally bounded variation on a (short) time-interval $I = [t_A, t_E]$ [16], the function $\boldsymbol{u}(t)$ admits a right $\boldsymbol{u}^+$ and left $\boldsymbol{u}^-$ limit for all $t \in I$, and its time-derivative $\dot{\boldsymbol{u}}$ exists for almost all $t \in I$. To be able to obtain $\boldsymbol{u}$ from integration we need to use the differential measure $\mathrm{d}\boldsymbol{u}$ where it is assumed that the measure can be decomposed into

$$\mathrm{d}\boldsymbol{u} = \dot{\boldsymbol{u}} \mathrm{d}t + \left( \boldsymbol{u}^+ - \boldsymbol{u}^- \right) \mathrm{d}\eta \tag{45}$$

where $\mathrm{d}t$ denotes the Lebesgue measure and $\mathrm{d}\eta$ denotes the atomic measure where $\int_{\{t_1\}} \mathrm{d}\eta = 1$.

From the notation above, the Newton-Euler equations as equality of measures can be written for the snake robot as

$$\mathbf{M}\mathrm{d}\boldsymbol{u} - \boldsymbol{h}(\boldsymbol{u})\mathrm{d}t - \mathrm{d}\boldsymbol{R} = \boldsymbol{\tau}_C \mathrm{d}t \tag{46}$$

where the mass matrix $\mathbf{M}$, the vector of smooth forces $\boldsymbol{h}(\boldsymbol{u})$, the force measure of possibly atomic impact impulsions $\mathrm{d}\boldsymbol{R}$, and the vector of applied torques $\boldsymbol{\tau}_C$ will be described in the following.

For our choice of coordinates, the mass matrix is *diagonal* and constant

$$\mathbf{M} = \begin{bmatrix} \mathbf{M}_1 & & \mathbf{0} \\ & \ddots & \\ \mathbf{0} & & \mathbf{M}_n \end{bmatrix} \in \mathbb{R}^{6n \times 6n} \tag{47}$$

with $\mathbf{M}_i = \mathrm{diag}\left( \begin{bmatrix} m_i & m_i & m_i & \Theta_{1i} & \Theta_{1i} & \Theta_{3i} \end{bmatrix} \right)$, $m_i$ is the mass of link $i$, and $\Theta_{1i}$ and $\Theta_{3i}$ are its moments of inertia. The smooth forces, here consisting of gravity and gyroscopic accelerations, are described by $\boldsymbol{h}(\boldsymbol{u}) = \begin{bmatrix} \boldsymbol{h}_1^{\mathrm{T}}(\boldsymbol{u}_1) & \cdots & \boldsymbol{h}_n^{\mathrm{T}}(\boldsymbol{u}_n) \end{bmatrix}^{\mathrm{T}} \in \mathbb{R}^{6n}$, where $\boldsymbol{h}_i(\boldsymbol{u}_i) = \begin{bmatrix} 0 & 0 & -m_i g & -({}_{B_i}\tilde{\boldsymbol{\omega}}_{IB_i} {}_{B_i}\boldsymbol{\Theta}_{G_i} {}_{B_i}\boldsymbol{\omega}_{IB_i})^{\mathrm{T}} \end{bmatrix}^{\mathrm{T}}$.

The force measure $\mathrm{d}\boldsymbol{R}$ accounts for all contact forces and impulses. The contact efforts that constitute $\mathrm{d}\boldsymbol{R}$ are found from the force-laws given in Section IV-B. Let $\mathcal{I}$ and $\mathcal{H}$ be the set of all active contacts with the ground and obstacles, respectively,

$$\mathcal{I}(t) = \{a \mid g_{N_a}(\boldsymbol{q}(t)) = 0\} \subseteq \{1, 2, \ldots, 2n\} \tag{48}$$
$$\mathcal{H}(t) = \{b \mid g_{H_b}(\boldsymbol{q}(t)) = 0\} \subseteq \{1, 2, \ldots, n\nu\} \tag{49}$$

where $g_{N_a}$ is the $a$-th element of the vector $\boldsymbol{g}_N$ in (14), and $g_{H_b}$ is $b$-th element of $\boldsymbol{g}_H$ in (12). Now, the force measure is written as

$$\mathrm{d}\boldsymbol{R} = \sum_{a \in \mathcal{I}} \left( (\mathbf{W}_N)_a \mathrm{d}\Lambda_{N_a} \right) + \mathbf{W}_J \mathrm{d}\boldsymbol{\Lambda}_J$$
$$+ \sum_{a \in \mathcal{I}} \left( (\mathbf{W}_T)_{2a-1} \mathrm{d}\Lambda_{T_{xa}} + (\mathbf{W}_T)_{2a} \mathrm{d}\Lambda_{T_{ya}} \right) \tag{50}$$
$$+ \sum_{b \in \mathcal{H}} (\mathbf{W}_H)_b \mathrm{d}\Lambda_{H_b}$$

where $\mathrm{d}\Lambda_{N_a}$ is the normal contact impulse measure between the ground and a link, $\mathrm{d}\boldsymbol{\Lambda}_J$ is the contact impulse measure due

to the bilateral constraints in the joints (these constraints are always active), $d\Lambda_{T_{xa}}$ and $d\Lambda_{T_{ya}}$ are the tangential contact impulse measures (friction) between the ground and a link, directed along $e_x^I$ and $e_y^I$, respectively, $d\Lambda_{H_b}$ is the normal contact impulse measure between a link and an obstacle, and the lower-case subscripts on the $\mathbf{W}$-matrices indicate which column of the matrix is used. The contact impulse measures are decomposed in the same way as for $d\boldsymbol{u}$ in (45). Let us take the normal contact impulse measure as an example. The measure can be written as

$$d\Lambda_{N_a} = \lambda_{N_a} dt + P_{N_a} d\eta \qquad (51)$$

where $\lambda_{N_a}$ is the Lebesgue-measurable force and $P_{N_a}$ is the purely atomic impact impulse. The same decomposition also holds for the other impulse measures.

Each cardan joint has 2 DOF that are controlled by two applied torques. For link $i$ we define a positive control torque $\tau_{v_i}$ to give a positive rotational velocity around $e_x^{B_{i+1}}$ and a positive control torque $\tau_{h_i}$ to give a positive rotational velocity around $e_y^{B_i}$. The total torque $\boldsymbol{\tau}_{C_i} \in \mathbb{R}^3$ applied to link $i$ is

$$
\begin{aligned}
\boldsymbol{\tau}_{C_i} &= \begin{bmatrix} 0 & \tau_{h_i} & 0 \end{bmatrix}^T - \mathbf{R}_{B_{i-1}}^{B_i} \begin{bmatrix} 0 & \tau_{h_{(i-1)}} & 0 \end{bmatrix}^T \\
&+ \mathbf{R}_{B_{i+1}}^{B_i} \begin{bmatrix} \tau_{v_i} & 0 & 0 \end{bmatrix}^T - \begin{bmatrix} \tau_{v_{(i-1)}} & 0 & 0 \end{bmatrix}^T
\end{aligned} \qquad (52)
$$

for $i = 1, \ldots, n$, where the relative rotation matrix is

$$\mathbf{R}_{B_{i+1}}^{B_i} = \left(\mathbf{R}_{B_i}^I\right)^T \mathbf{R}_{B_{i+1}}^I, \qquad (53)$$

and $\tau_{h_0} = \tau_{v_0} = \tau_{h_n} = \tau_{v_n} = 0$.

The vector of the torques applied to all links $\boldsymbol{\tau}_C \in \mathbb{R}^{6n}$ is

$$\boldsymbol{\tau}_C = \begin{bmatrix} \mathbf{0}_{1\times3} & \boldsymbol{\tau}_{C_1}^T & \mathbf{0}_{1\times3} & \boldsymbol{\tau}_{C_2}^T & \cdots & \mathbf{0}_{1\times3} & \boldsymbol{\tau}_{C_n}^T \end{bmatrix}^T. \qquad (54)$$

### B. Constitutive Laws for the Contact Forces

In this section, we introduce set-valued force laws for normal contact with the ground and obstacles, and Coulomb friction. These laws will all be formulated on velocity level using the relative contact velocities $\gamma$ given by (27), (33), and (38). Subsequently, the set-valued force laws are formulated as equalities in Section IV-B.3 using the so-called 'proximal point function' in order to include the force laws in the numerical simulation [12].

*1) Normal Contact Force:* The normal contact between a link and the ground or an obstacle is described by the condition

$$\gamma_N \geq 0, \ \lambda_N \geq 0, \quad \gamma_N \lambda_N = 0, \qquad (55)$$

for a closed contact $g_N = 0$, where $\lambda_N$ is the normal contact force, $\gamma_N$ is the relative velocity, and $g_N$ is the gap function. The condition (55) is equivalent to the inclusion

$$-\gamma_N \in N_{C_N}(\lambda_N), \qquad (56)$$

where the convex set $C_N = \{\lambda_N \mid \lambda_N \geq 0\} = \mathbb{R}^+$ is the set of admissible contact forces, and $N_{C_N}$ is the normal cone to $C_N$ (see [10], [12]). This force law describes the impenetrability of sustained contact, i.e. $g_N = 0$ and $\gamma_N = 0$, as well as detachment: $\gamma_N > 0 \Rightarrow \lambda_N = 0$. The force law (56) only covers finite-valued contact efforts during impulse
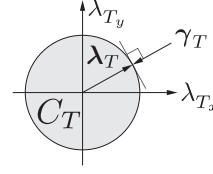


Fig. 5. Relationship between tangential relative velocity and friction force. The set $C_T$ is in grey.

free motion, i.e. all velocities are locally absolutely continuous in time. When a collision occurs in a rigid-body setting, then the velocities will be locally discontinuous in order to prevent penetration. The velocity jump is accompanied by an impact impulse $P_N$, for which we will set up an impact law. The relative velocity admits, similarly to the velocities $\boldsymbol{u}$, a right $\gamma_N^+$ and a left $\gamma_N^-$ limit. The impact law for a completely inelastic impact at a closed contact can now be written as

$$-\gamma_N^+ \in N_{C_N}(P_N), \quad C_N = \{P_N \mid P_N \geq 0\} = \mathbb{R}^+. \quad (57)$$

*2) Coulomb Friction Force:* Similarly to the force law (56) for normal contact, we describe the constitutive description for friction using an inclusion on a normal cone. The friction force $\boldsymbol{\lambda}_T$ between the ground and a link, in the two-dimensional tangent plane to the contact point, is modeled with an isotropic Coulomb friction law

$$-\boldsymbol{\gamma}_T \in N_{C_T}(\boldsymbol{\lambda}_T), \qquad (58)$$

where $\boldsymbol{\gamma}_T$ is a relative sliding velocity, $C_T = \{\boldsymbol{\lambda}_T \mid \|\boldsymbol{\lambda}_T\| \leq \mu_T \lambda_N\}$ is the set of admissible friction forces, $\mu_T > 0$ is the friction coefficient, and $N_{C_T}$ is the normal cone to the set $C_T$ (see Fig. 5). The set-valued force law (58) contains to the cases of stick and slip

$$
\begin{array}{llll}
\text{stick}: & \boldsymbol{\gamma}_T = \mathbf{0}, & \|\boldsymbol{\lambda}_T\| \leq \mu_T \lambda_N & \\
\text{slip}: & \boldsymbol{\gamma}_T \neq \mathbf{0}, & \boldsymbol{\lambda}_T = -\mu_T \lambda_N \frac{\boldsymbol{\gamma}_T}{\|\boldsymbol{\gamma}_T\|} &
\end{array} \qquad (59)
$$

The advantage of formulating the friction law as the inclusion (58) now becomes apparent. A spatial friction law such as (58), which is equivalent to (59), can not properly be described by a set-valued sign-function. Some authors model the spatial contact with two sign-functions for the two components of the relative sliding velocity using two friction coefficients $\mu_{T_x}$ and $\mu_{T_y}$ [8], [17]. This results however directly in an anisotropic friction law, as the friction force and the sliding velocity do no longer point in opposite directions. If indeed *set-valued* sign-functions are chosen, then such a double-sign-function force law corresponds to (58) with $C_T$ being a rectangle with length $\mu_{T_x} \lambda_N$ and width $\mu_{T_y} \lambda_N$. Also, the (set-valued) sign function can be approximated with a smoothening function, for example some arctangent function. This results in a very steep slope of the friction curve near zero relative velocity. Such an approach is very cumbersome for two reasons. First of all, stiction can not properly be described: an object on a slope will with a smoothened friction law always slide. Secondly, the very steep slope of the friction curve causes the differential equations of motion to become

numerically stiff. Summarising, we see that (58) or (59) describes spatial Coulomb friction taking isotropy and stiction properly into account. We prefer using (58) instead of (59), because the latter becomes not well conditioned for very small $\gamma_T$ when used in numerics. Note also that (58) and (56) have the same mathematical form. Moreover, the inclusion (58) is much more general since we can easily change the convex set $C_T$ to get a different (and hence anisotropic) friction model.

*3) Constitutive Laws as Projections:* An inclusion can not be directly employed in numerical calculations. Hence, we transform the force laws (56) and (58), which have been stated as an inclusion to a normal cone, into an equality. This is achieved through the so-called proximal point function $\text{prox}_C(\boldsymbol{x})$, which equals $\boldsymbol{x}$ if $\boldsymbol{x} \in C$ and equals the closest point in $C$ to $\boldsymbol{x}$ if $\boldsymbol{x} \notin C$. The set $C$ must be convex. Using the proximal point function we transform the force laws into implicit equalities (see [12])

$$-\gamma_\kappa \in N_{C_\kappa}(\lambda_\kappa) \iff \lambda_\kappa = \text{prox}_{C_\kappa}(\lambda_\kappa - r_\kappa \gamma_\kappa), \quad (60)$$

where $r_\kappa > 0$ for $\kappa = N, T$.

## V. MOTION PATTERN AND JOINT CONTROL

In this section, we will define the joint angles and show how to control them for snake robot locomotion.

### A. Control of the Joint Angles

The joint angles are not directly accessible from the non-minimal coordinates, but can be calculated from the relative rotation matrices $\mathbf{R}^{B_i}_{B_{i+1}}$ in (53) (see [10]). Let $\alpha_{vi}$ and $\alpha_{hi}$ be the two joint angles in the cardan joint between link $i$ and $i+1$. We define $\boldsymbol{e}^{B_{i+1}}_x$ and $\boldsymbol{e}^{B_i}_y$ to be the axis of rotation for $\alpha_{vi}$ and $\alpha_{hi}$, respectively. We define $\alpha_{vi} = \alpha_{hi} = 0$ for the case when link $i$ and $i+1$ are parallel.

Let the desired values of $\alpha_{h_i}$ and $\alpha_{v_i}$ be $\alpha_{h_i,r}$ and $\alpha_{v_i,r}$, respectively. Then, the proportional-derivative controllers (PD-control) for the joints are chosen to be

$$\tau_{h_i} = K_{h,p}(\alpha_{h_i} - \alpha_{h_i,r}) - K_{h,d}(_{B_i}\boldsymbol{\omega}_{IB_i})_2 \quad (61)$$

$$\tau_{v_i} = K_{v,p}(\alpha_{v_i} - \alpha_{v_i,r}) + K_{v,d}(_{B_{i+1}}\boldsymbol{\omega}_{IB_{i+1}})_1 \quad (62)$$

for $i = 1, \ldots, n-1$ where $K_{h,p}$, $K_{h,d}$, $K_{v,p}$, and $K_{v,d}$ are constants and equal for all $i$, and the subscripts $_2$ and $_1$ denote the second and first element of their respective vectors.

### B. Motion Pattern and Reference Angles

The motion pattern lateral undulation [3] is typical for biological and robot snakes and has been implemented in this paper. Snakes use this for locomotion by propagating horizontal waves from the front to the rear of the snake body while exploiting roughness in the terrain. In this paper, cylindrical obstacles are introduced to model the roughness in the terrain.

The desired joint angles for lateral undulation are

$$\alpha_{h_i,r} = A_h \sin(\omega_h t + (i-1)\delta_h) + \psi_h, \quad (63)$$

and $\alpha_{v_i,r} = 0$ for $i = 1, \ldots, n-1$, where $A_h$ is the amplitude of joint oscillation, $\omega_h$ is the angular frequency, $\delta_h$ is the phase offset, and $\psi_h$ controls the direction of motion [6], [8].

## VI. NUMERICAL ALGORITHM - TIME-STEPPING

The numerical solution to the equality of measures is found with an algorithm called the time-stepping-method introduced in [16] (See also [12], [14]).

The implementation of the time-stepping-method for the snake robot without external obstacles is described in [10]. The obstacle contact forces and impulses are included in the numerical solution the same way as the ground contact forces and impulses. A short description of the algorithm is given as follows: Select a time-step size $\Delta t$ and consider the time-interval $I = [t_A, t_E]$ where $t_E - t_A = \Delta t$. Calculate the states at the mid-point $t_M = t_A + \frac{1}{2}\Delta t$ and use these to find the approximation of the gyroscopic forces $\boldsymbol{h}_M$, and the directions of the various forces and impulses that act during the time-interval. These directions are given by the matrices $\mathbf{W}_\Xi$, where $\Xi = N, T, H, J$, Then, employ the Modified Newton Algorithm [18] to find the forces and impulses involved in the active contact points together with the velocities at $t_E$ that are found from the equality of measures. Finally, the positions at the end of the time-interval (at $t_E$) can be found by integrating over the latter half part of the time-step $\Delta t$.

## VII. NUMERICAL RESULTS

In this section, we demonstrate that the non-smooth model developed in this paper works for obstacle aided locomotion.

### A. System and Simulation Parameters

The choice of parameters used to describe the snake robot is based on the water-hydraulic based snake robot built by the Norwegian research organisation Sintef in Trondheim [19]. The model parameters are: $n = 11$ links, $L_i = 0.269$ m, $L_{SC} = 0.0795$ m, $L_{GS_i} = 0.1016$ m, $m_i = 7$ kg, $\Theta_{1i} = 0.0450$ kg m$^2$, $\Theta_{3i} = 0.0055$ kg m$^2$, $i = 1, \ldots, 11$, and the PD-controllers are implemented with the gains $K_{h,p} = 400$ Nm, $K_{h,d} = 20$ Nm, $K_{v,p} = 200$ Nm, and $K_{v,d} = 10$ Nm. The simulation parameters are $r_H = r_N = 2$, $r_T = 0.5$, and $\Delta t = \frac{t_{\text{stop}} - t_{\text{start}}}{N-1}$, where $N$ is the number of integration steps, and $t_{\text{start}}$ and $t_{\text{stop}}$ is the start and stop time of the simulation, respectively. The friction coefficient is $\mu_T = 0.05$. The radii $(L_j)$ of the obstacles 1 to $\nu = 10$ are (in metres): 0.05, 0.2, 0.02, 0.05, 0.3, 0.05, 0.2, 0.1, 0.05, 0.25, respectively. The serpentine motion pattern lateral undulation was implemented with $A_h = 30\pi/180$, $\omega_h = 60\pi/180$, $\delta_h = 50\pi/180$, and $\psi_h = 0$.

### B. Simulation Result

The snake robot is set to move along the $\boldsymbol{e}^I_x$-axis with lateral undulation using external obstacles. The obstacles are placed along the estimated path of the snake robot. Illustrations of the snake robot during simulation are given in Fig. 6.

The snake robot is positioned along the $\boldsymbol{e}^I_x$-axis. Fig. 7 shows the position $(x_{CG}, y_{CG})$ in the $(\boldsymbol{e}^I_x, \boldsymbol{e}^I_y)$-plane of the centre of gravity of the snake robot. We see that the snake robot is able to move forward using only the obstacles to push against.
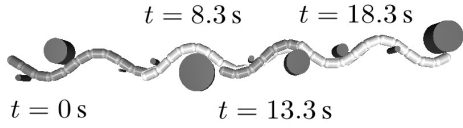
Fig. 6. Snake robot during lateral undulation at four points in time.

## VIII. CONCLUSION AND FURTHER WORK

An analytical model of a snake robot with external obstacles has been developed in this paper. Such a model can be used for both analysis of obstacle aided locomotion based on the equality of measures, and simulations of locomotion. Usually, the serpentine motion pattern lateral undulation is implemented on snake robots that have an anisotropic friction property with the ground. This is because without this property, the snake robots would hardly be able to move forward. In this paper, we have used an isotropic friction model and included obstacles that the snake robot could push against. This made the snake robot independent of the anisotropic friction property for locomotion. Hence, the locomotion is less dependent on the surface properties of the ground.

It has been shown how to easily and systematically incorporate the various contact forces into the equality of measures by set-valued force laws. In fact, the hardest part in the modelling is finding the shortest distance between the two bodies under consideration.

The contact between a link and an obstacle is modeled with a single contact point that may move over the entire surface of the link. This approach can also be employed for modeling robot manipulators that come into contact with its environment. The moving contact point gives us an accurate description of how the contact with an obstacle affects the torque around the centre of gravity (CG) of a link. Also, it allows for cylindrical obstacles of *any* (strictly positive) radius without having to worry about the snake robot getting stuck during locomotion, or that the obstacle just goes through the robot (both as for the case when only the CG is used as a possible contact point).
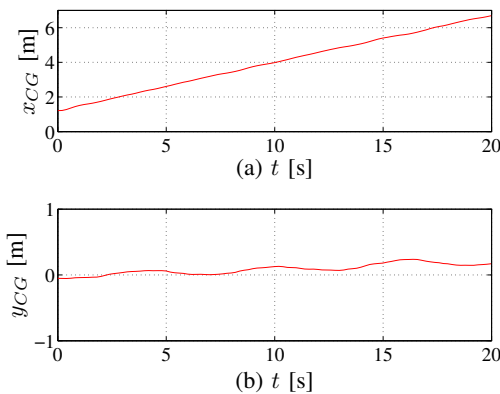


Fig. 7. Positions of the CG of the snake robot (a) along the $\boldsymbol{e}_x^I$-axis ($x_{CG}$) and (b) along the $\boldsymbol{e}_y^I$-axis ($y_{CG}$).

The choice of non-minimal absolute coordinates resulted in a constant and diagonal mass matrix, and a simple expression for the gyroscopic forces. The coordinates are no longer minimal with respect to the bilateral constraints and yield in the absence of unilateral forces a differential algebraic equation (DAE). However this is not a real complication, as we already need a Lagrangian multiplier description for the frictional unilateral contact forces.

Suggestions for further research are: 1) include friction in the contact between the snake robot and the obstacles, and 2) develop snake robot motion patterns for both planar and 3D motion where the snake robot utilizes external obstacles to optimize for terrainability and locomotion speed.

## REFERENCES

[1] J. Gray, "The mechanism of locomotion in snakes," *J. Exp. Biol.*, vol. 23, no. 2, pp. 101–120, 1946.
[2] S. Hirose and Y. Umetani, "Kinematic control of active cord-mechanism with tactile sensors," in *Proc. 2nd RoMAnSy Symp.*, Warsaw, 1976, pp. 241–252.
[3] S. Hirose, *Biologically Inspired Robots: Snake-Like Locomotors and Manipulators*. Oxford: Oxford University Press, 1993.
[4] Z. Bayraktaroglu and P. Blazevic, "Understanding snakelike locomotion through a novel push-point approach," *J. Dyn. Syst. - Trans. ASME*, vol. 127, no. 1, pp. 146–152, March 2005.
[5] S. Ma, Y. Ohmameuda, and K. Inoue, "Dynamic analysis of 3-dimensional snake robots," in *Proc. IEEE/RSJ Int. Conf. On Intelligent Robots and Systems*, 2004, pp. 767–772.
[6] P. Liljebäck, Ø. Stavdahl, and K. Y. Pettersen, "Modular pneumatic snake robot: 3D modelling, implementation and control," in *Proc. 16th IFAC World Congress*, July 2005.
[7] B. Brogliato, *Nonsmooth Mechanics*, 2nd ed. London: Springer, 1999.
[8] M. Saito, M. Fukaya, and T. Iwasaki, "Serpentine locomotion with robotic snakes," *IEEE Contr. Syst. Mag.*, vol. 22, no. 1, pp. 64–81, February 2002.
[9] K. McIsaac and J. Ostrowski, "Motion planning for anguilliform locomotion," *IEEE Trans. Robot. Autom.*, vol. 19, no. 4, pp. 637–625, August 2003.
[10] A. A. Transeth, R. I. Leine, Ch. Glocker, and K. Y. Pettersen, "Non-smooth 3D modeling of a snake robot with frictional unilateral constraints," in *Proc. IEEE/RSJ Int. Conf. Robotics and Biomimetics*, Dec 2006.
[11] Ch. Glocker, *Set-Valued Force Laws, Dynamics of Non-Smooth Systems*, ser. Lecture Notes in Applied Mechanics. Berlin: Springer-Verlag, 2001, vol. 1.
[12] R. I. Leine and H. Nijmeijer, *Dynamics and Bifurcations of Non-Smooth Mechanical Systems*, ser. Lecture Notes in Applied and Computational Mechanics. Berlin: Springer Verlag, 2004, vol. 18.
[13] O. Egeland and J. T. Gravdahl, *Modeling and Simulation for Automatic Control*. Trondheim, Norway: Marine Cybernetics, 2002.
[14] Ch. Glocker and C. Studer, "Formulation and preparation for numerical evaluation of linear complementarity systems in dynamics," *Multibody System Dynamics*, vol. 13, pp. 447–463, 2005.
[15] C. Le Saux, R. I. Leine, and Ch. Glocker, "Dynamics of a rolling disk in the presence of dry friction," *Journal of Nonlinear Science*, vol. 15, no. 1, pp. 27–61, 2005.
[16] J. J. Moreau, "Unilateral contact and dry friction in finite freedom dynamics," in *Non-Smooth Mechanics and Applications*, ser. CISM Courses and Lectures, J. J. Moreau and P. D. Panagiotopoulos, Eds. Wien: Springer Verlag, 1988, vol. 302, pp. 1–82.
[17] S. Ma, N. Tadokoro, B. Li, and K. Inoue, "Analysis of creeping locomotion of a snake robot on a slope," in *Proc. IEEE Int. Conf. Robotics and Automation*, September 2003, pp. 2073–2078.
[18] P. Alart and A. Curnier, "A mixed formulation for frictional contact problems prone to Newton like solution methods," *Comput. Method. Appl. M.*, vol. 92, pp. 353–375, 1991.
[19] P. Liljebäck, Ø. Stavdahl, and A. Beitnes, "SnakeFighter. development of a water hydraulic fire fighting snake robot," in *Proc. IEEE Int. Conf. Control, Automation, Robotics, and Vision*, Dec 2006.